J. Plasma Physics (2001), *vol.* 65, *part* 3, *pp.* 213–233. © 2001 Cambridge University Press
DOI: 10.1017/S0022377801001076 Printed in the United Kingdom

Nonlinear waves propagating transverse to the magnetic field

J. F. McKENZIE,[1,2] E. DUBININ[1,3] and K. SAUER[1]

[1]Max Planck Institut für Aeronomie, Katlenburg–Lindau, Germany

[2]School of Pure and Applied Physics, University of Natal, Durban, South Africa

[3]Centre d'Etude des Environnements Terrestre et Planetaires, Velizy, France

(Received 6 March 2001)

Abstract. We generalize the classical work of Adlam and Allen [*Phil. Mag.* **3**, 448 (1958)] on solitons in a cold plasma propagating perpendicular to the magnetic field to include the effects of plasma pressure. This is done by making extensive use of the properties of total momentum conservation (denoted by the term 'momentum hodograph', since it yields a locus in the plane of the electron and proton speeds in the direction of the wave) and the energy integral of the system as a whole. These relations elucidate the phase and integral curves of stationary flows, from which soliton solutions may be constructed. In general, only compressive solitons are permitted, and we have found an analytical expression for the critical fast Mach number as a function of the proton acoustic Mach number, which shows that it varies from its classical value of 2 (at large proton acoustic Mach numbers) to unity, where the incoming flow is proton-sonic. At the critical fast Mach number, two possible soliton-like solutions can be constructed. One is the classical compression, in which the magnetic field develops a cusp in the centre of the wave. The other is a compression in the magnetic field followed by a deep depression in the centre of the wave, which is completed by the mirror image of this signature of compression–rarefaction. This structure involves a smooth supersonic–subsonic transition in the proton flow. For Mach numbers in excess of the critical one, this kind of structure can also be constructed, but now the magnetic field is cusp-like at the points of maximum compression.

1. Introduction

The intrinsic properties of nonlinear waves in a magnetized plasma shed light on how solitary waves (solitons) (see e.g. Karpman 1975; Drazin 1983) are constructed and how these in turn may be used in the theory of the structure of collisionless shocks (see e.g. Kennel et al. 1985). In this paper, we generalize the classical work of Adlam and Allen (1958), Vedenov et al. (1961) and Sagdeev (1966) to include the effect of plasma pressure, which, as we shall see, can have a dramatic influence. We consider only stationary waves propagating perpendicular to the magnetic field, so that the natural length scale appearing in the system is a lower-hybrid one based on the Alfvén speed divided by the lower hybrid frequency by virtue of the fact that in the wave proton deflections of the flow are balanced by correspondingly large deflections in the electron flow.

Our approach makes extensive use of the conservation of the fluxes of total

https://doi.org/10.1017/S0022377801001076 Published online by Cambridge University Press

momentum and energy of the system as a whole in a frame in which the waves appear stationary. Momentum conservation can be cast as an algebraic relation between the electron speed in the direction of the wave, u_e say (or magnetic field strength), and its proton counterpart u_p. We call this the momentum hodograph of the system, and we show how its locus in the (u_p, u_e) plane depends on the fast Mach number M_f and the proton acoustic Mach number M_p. The differential equation for the structure of the wave represents conservation of total energy flux of the system. This structure equation, along with the hodograph, enables us to construct the phase and integral curves, which in turn are used to construct soliton solutions. A necessary condition for such stationary waves to exist is that the flow must be either superfast ($M_f > 1$) or sub-proton-acoustic ($M_p < 1$). This follows from the linearized structure equation by demanding that the waves be of the evanescent type (growing or decaying) at the ends of the structure.

It is shown that only compressive solitons are permitted, and we find an analytical expression for the critical fast Mach number as a function of the proton acoustic Mach number that shows that it goes from the classical value of 2 for $M_p \to \infty$, to unity as $M_p \to 1$. Thus proton-pressure effects reduce the critical fast Mach number. At this critical fast Mach number, there are two possible solutions for the structure of the critical soliton. One is the classical compression of the magnetic field, where the magnetic field is cusp-like at the centre of the wave. The other possibility is a compression in the magnetic field followed by a deep depression, with the recovery to the initial state being the mirror image reflected about the centre of the wave. This type of transition involves a supersonic–subsonic transition in the proton flow, which takes place where the magnetic field reaches its maximum value. Thus the centre of the wave is characterized by a hole in the magnetic field accompanied by low proton speed (and high electron speed) and high proton pressure. At Mach numbers in excess of the critical one, a similar structure may be constructed, but this involves cusp-like behaviour of the magnetic field at its maximum compression. Whether these structures can stably exist is a moot point.

Finally, it is noteworthy that we can construct structures involving a plasma subshock in a manner similar to the insertion of a gas subshock in the theory of cosmic-ray shocks (Axford et al. 1982) and in theory of collisionless shocks (see e.g. Kennel et al. 1985).

The layout of the paper is as follows. The governing equations are given in the next section, in which we derive the constants of the motion. In Sec. 3, we specialize to the case of flow transverse to the magnetic field, and derive the structure equation for the system, which at this stage is a second-order differential equation for the proton flow speed u_{px}. The stationary-wave dispersion relation is obtained in Sec. 4 by linearizing the second-order structure equation. We see here that evanescent stationary waves are only possible if $M_f > 1$ or $M_p < 1$. In Sec. 5, we discuss the properties of the momentum hodograph. The energy integral of the system is derived in Sec. 6, in which we recapitulate the properties of the cold soliton of Adlam and Allen (1958). In Sec. 7, we discuss the effects of plasma pressure on the phase and integral curves and derive the various properties and structures to which we have already alluded.

2. Governing equations

In a magnetized plasma consisting of protons (p) and electrons (e), the fluid equations for each constituent and the Maxwell equations combine to yield total

https://doi.org/10.1017/S0022377801001076 Published online by Cambridge University Press

momentum conservation in the form

$$\sum_{i=p,e} m_i n_i \frac{D_i \mathbf{u}_i}{Dt} + \boldsymbol{\nabla}\left(p_p + p_e + \frac{B^2}{2\mu_0} + \frac{\varepsilon_0 E^2}{2}\right) - \frac{\mathbf{B}\cdot\boldsymbol{\nabla}\mathbf{B}}{\mu_0}$$

$$-\varepsilon_0 \mathbf{E}\cdot\boldsymbol{\nabla}\mathbf{E} - \varepsilon_0 \mathbf{E}\boldsymbol{\nabla}\cdot\mathbf{E} = -\frac{1}{c^2}\frac{\partial}{\partial t}\left(\frac{\mathbf{E}\times\mathbf{B}}{\mu_0}\right), \tag{1a}$$

in which the convective derivative

$$\frac{D_i}{Dt} = \frac{\partial}{\partial t} + \mathbf{u}_i\cdot\boldsymbol{\nabla} \tag{1b}$$

and m_i is the mass ($i = p$ for protons, $i = e$ for electrons), n_i is the number density, p_i is the pressure of each constituent, $\mathbf{B} = (B_x, B_y, B_z)$ is the magnetic field and $\mathbf{E} = (E_x, E_y, E_z)$ is the electric field. Mass conservation for each species takes the usual form

$$\frac{D_i(m_i n_i)}{Dt} + \mathbf{u}_i\cdot\boldsymbol{\nabla}(m_i n_i) = 0. \tag{2}$$

The Reynold stresses are bound up in the inertial terms (the first term on the left-hand side of (1a)); the plasma pressure and the Maxwell stresses are evident in the pressure and tension terms, with the sum of all these stresses being balanced by the time rate of change of the momentum associated with the Poynting vector $\mathbf{E}\times\mathbf{B}/\mu_0$ on the right hand side. In seeking solutions that are stationary in a frame moving with speed V along the x axis (say), i.e. quantities vary only with $\xi = x - Vt$, the convective derivative becomes

$$\frac{D_i}{Dt} = (u_{ix} - V)\frac{d}{d\xi}. \tag{3}$$

The continuity equation integrates immediately to

$$m_i n_i (u_{ix} - V) = \text{const} = \mathscr{M}_i, \quad \text{say.} \tag{4}$$

It is convenient to perform the subsequent analysis in a frame in which $V = 0$, so that in this frame, we consider a stationary flow ($\partial/\partial t = 0$) with only spatial variations in $x (d/d\xi = d/dx)$. In this frame, Faraday's law tells us that

$$E_y = \text{const}, \qquad E_z = \text{const}, \tag{5}$$

and Gauss's law gives

$$B_x = \text{const}. \tag{6}$$

The momentum equation integrates immediately to yield the conservation of the three components of the momentum flux, namely

$$\mathscr{M}_p u_{px} + \mathscr{M}_e u_{ex} + p_p + p_e + \frac{B_z^2 + B_y^2}{2\mu_0} - \frac{\varepsilon_0 E_x^2}{2} = \mathscr{F}_x, \quad \text{const}, \tag{7a}$$

$$\mathscr{M}_p u_{py} + \mathscr{M}_e u_{ey} - \frac{B_x B_y}{\mu_0} - \varepsilon_0 E_x E_y = \mathscr{F}_y, \quad \text{const}, \tag{7b}$$

$$\mathscr{M}_p u_{pz} + \mathscr{M}_e u_{ez} - \frac{B_x B_z}{\mu_0} - \varepsilon_0 E_x E_z = \mathscr{F}_z, \quad \text{const}. \tag{7c}$$

The equations of motion for each constituent are

$$m_i n_i \frac{D_i \mathbf{u}_i}{Dt} = e n_i (\mathbf{E} + \mathbf{u}_i \times \mathbf{B}) - \boldsymbol{\nabla} p_i, \tag{8}$$

https://doi.org/10.1017/S0022377801001076 Published online by Cambridge University Press

with

$$\frac{D_i}{Dt} = u_i \frac{d}{dx}, \qquad \boldsymbol{\nabla} = \mathbf{x}\frac{d}{dx}.$$

The system is completed with an energy equation, which, if dissipation is negligible, may be replaced with the condition of adiabatic flow

$$p_i \propto n_i^{\gamma i} \propto u_{ix}^{-\gamma i}. \tag{9a}$$

This provides an isentropic sound speed c_i for each constituent, given by

$$c_i^2 = \frac{1}{m_i}\frac{dp_i}{dn_i} = \frac{\gamma_i p_i}{m_i n_i} \propto u_{ix}^{-(\gamma_i - 1)}. \tag{10}$$

3. Flow transverse to the magnetic field

We now consider the special case of proton–electron flow transverse to the magnetic field by taking the configuration

$$\mathbf{u}_i = (u_{ix}, u_{iy}, 0), \qquad \mathbf{B} = (0, 0, B_z). \tag{11}$$

In the electron equation of motion, we consider the electron inertia to be negligible, so that

$$\mathbf{E} = -\mathbf{u}_e \times \mathbf{B} - \frac{\boldsymbol{\nabla} p_e}{e n_e}, \tag{12}$$

which, along with Faraday's law (5), yields

$$E_y = u_{ex} B_z = \text{const}, \tag{13a}$$

$$E_z = 0, \tag{13b}$$

$$E_x = -u_{ey} B_z - \frac{1}{e n_e}\frac{dp_e}{dx}. \tag{13c}$$

The x and y components of the proton equation of motion become

$$\frac{1}{\Omega_p}\frac{D_p u_{px}}{Dt} = u_{py} - u_{ey} - \frac{1}{m_p \Omega_p}\left(\frac{1}{n_p}\frac{dp_p}{dx} + \frac{1}{n_e}\frac{dp_e}{dx}\right), \tag{14a}$$

$$\frac{1}{\Omega_p}\frac{D_p u_{py}}{Dt} = u_{ex} - u_{px}, \tag{14b}$$

in which

$$\Omega_p = \frac{e B_z}{m_p} \tag{15}$$

is the proton gyrofrequency. The x component of total momentum approximates to

$$\mathscr{M}_p u_{px} + p_p + p_e + \frac{B_z^2}{2\mu_0} - \frac{\varepsilon_0 E_x^2}{2} = \mathscr{F}_x, \tag{16}$$

since $\mathscr{M}_e u_{ex}$ is smaller than $\mathscr{M}_p u_{px}$ by the mass ratio m_e/m_p by virtue of $n_e u_{ex} = n_p u_{px}$, which follows from zero current in the x direction. However, in the y component of the total momentum, we retain the electron inertia component because it permits a small deflection of the proton flow in the y direction, that is

$$\mathscr{M}_p u_{py} = -\mathscr{M}_e u_{ey}, \tag{17a}$$

https://doi.org/10.1017/S0022377801001076 Published online by Cambridge University Press

or

$$u_{py} = -\frac{m_e}{m_p} u_{ey} \tag{17b}$$

if the undisturbed flow has zero y momentum. Thus, in (14a), we may neglect u_{py} compared with u_{ey} on the right-hand side, and also rewrite (14b) in the form

$$-\frac{1}{\Omega_e}\frac{D_p u_{ey}}{Dt} = u_{ex} - u_{px}, \tag{18}$$

in which Ω_e is the electron gyrofrequency. Equations (14a) and (18) combine to yield, after elimination of u_{ey},

$$\frac{1}{\Omega_e}\frac{D_p}{Dt}\left\{\frac{1}{\Omega_p}\left[\frac{D_p u_{px}}{Dt} + \frac{1}{m_p}\left(\frac{1}{n_e}\frac{dp_e}{dx} + \frac{1}{n_p}\frac{dp_p}{dx}\right)\right]\right\} = u_{ex} - u_{px}. \tag{19a}$$

Using the adiabatic relations to eliminate p_e and p_p in terms of u_{ex} and u_{px}, this equation may be written in the form

$$\frac{1}{\Omega_e} u_{px}\frac{d}{dx}\left\{\frac{1}{\Omega_p}\left[\left(u_{px} - \frac{c_p^2}{u_{px}}\right)\frac{du_{px}}{dx} - \frac{c_e^2}{u_{ex}}\frac{du_{ex}}{dx}\right]\right\} = u_{ex} - u_{px}, \tag{19b}$$

in which the sound speeds c_p and c_e are given by

$$c_p^2 = \frac{\gamma_p p_p}{m_p n_p}, \qquad c_e^2 = \frac{\gamma_e p_e}{m_p n_e}. \tag{20}$$

With E_x given by (13c), it is clear that the electric tension term $\frac{1}{2}\varepsilon_0 E_x^2$ is relativistically small compared with the magnetic pressure $B^2/2\mu_0$ in the x component of momentum, (16), which therefore approximates to

$$\mathscr{M}_p u_{px} + p_p + p_e + \frac{B_z^2}{2\mu_0} = \mathscr{F}_x. \tag{21}$$

By virtue of the adiabatic relations and (13a) (which tells us that the magnetic field is frozen into the electrons and that its pressure is equivalent to an adiabatic relation with $\gamma = 2$), the momentum equation (21) provides a relation between u_{ex} and u_{px}, which we call the momentum hodograph. We can use this relation to eliminate u_{ex} from (19b) to obtain

$$\frac{1}{\Omega_e} u_{px}\frac{d}{dx}\left[\frac{1}{\Omega_p}\left(1 - \frac{c_p^2}{u_{px}^2}\right)\frac{V_A^2}{c_e^2 + V_A^2} u_{px}\frac{du_{px}}{dx}\right] = u_{ex} - u_{px}, \tag{22}$$

where we have used

$$\frac{1}{u_{ex}}\frac{du_{ex}}{dx} = \frac{1 - c_p^2/u_{px}^2}{c_e^2 + V_A^2} u_{px}\frac{du_{px}}{dx}, \tag{23}$$

which follows from (21) regarded as determining $u_{ex} = f(u_{px})$. It is important to note that although we have neglected the electric stresses in the momentum conservation, we do not insist on charge neutrality ($n_e = n_p$) – if we had done so, this would have implied $u_{ex} = u_{px}$, which in turn would have violated conservation of momentum except for very small-amplitude disturbances.

Equation (22) is the structure equation for stationary flows (or waves) transverse to a magnetic field. It is a second-order, highly nonlinear equation for u_{px} as a function of the spatial coordinate x. At this stage, it does not appear to be amenable to fruitful analytical development, but, as we shall subsequently see, it is possible

https://doi.org/10.1017/S0022377801001076 Published online by Cambridge University Press

to obtain a first integral that combined with the momentum hodograph, enables us to elucidate the flow patterns and magnetic field variations that can arise in stationary transverse waves (solitons).

4. Stationary-wave dispersion equation (condition for solitons)

The dispersion equation for stationary waves may be obtained from linearizing the structure equation about some initial state where the flow speed is $u_{px} = u_0$ and the magnetic field is B_0 and seeking exponential solutions $\exp(\kappa x)$, which immediately yields the exponent κ from

$$\kappa^2 = \frac{\Omega_{p0}\Omega_{e0}}{V_{A0}^2}\,\frac{u_0^2 - (c_e^2 + c_p^2 + V_A^2)_0}{u_0^2 - c_{p0}^2}. \tag{24a}$$

The condition $\kappa^2 > 0$ (which implies that the waves are of the evanescent type, i.e. either growing or decaying) means that solitons may exist if the flow speed is either sub-proton-acoustic or superfast:

$$u_0 < c_{p0} \quad \text{or} \quad u_0 > (c_{e0}^2 + c_{p0}^2 + V_{A0}^2)^{1/2} = V_{f0}. \tag{24b}$$

Figure 1(a) shows the variation of κ with speed u_0. Propagating solutions of the form $\exp[i(\omega t - kx)]$ may be extracted from (24a) by the transformations

$$\kappa \to -ik, \qquad u_0 = V_{\rm ph} = \frac{\omega}{k}, \tag{25a}$$

giving

$$V_{\rm ph}^2 = \frac{V_{f0}^2 + \dfrac{c_{p0}^2 V_{A0}^2 k^2}{\Omega_{p0}\Omega_{e0}}}{1 + \dfrac{V_{A0}^2 k^2}{\Omega_{p0}\Omega_{e0}}}. \tag{25b}$$

Thus the phase speed equals the fast speed V_{f0} at long wavelengths ($k \to 0$), and decreases with increasing k (going through a quasiresonance where $\omega \sim \sqrt{\Omega_{p0}\Omega_{e0}}$), asymptotically approaching the proton acoustic speed c_{p0} for very short wavelengths ($V_A k/\sqrt{\Omega_{p0}\Omega_{e0}} \gg 1$). These properties are depicted in Figs 1(b) and 1(c), where in the latter the hatched region corresponds to where $V_{\rm ph}$ is imaginary and therefore indicates the region where soliton solutions may exist according to (24b).

5. The momentum hodograph

All solutions of the structure equation (22) lie on a locus in the phase plane (u_{ex}, u_{px}) defined by the conservation of the x component of total momentum, (21), which in normalized form may be written as

$$u_p - 1 + \frac{1}{\gamma_p M_p^2}\left(\frac{1}{u_p^{\gamma_p}} - 1\right) = \frac{1}{\gamma_e M_e^2}\left(1 - \frac{1}{u_e^{\gamma_e}}\right) + \frac{1}{2M_A^2}\left(1 - \frac{1}{u_e^2}\right), \tag{26}$$

in which

$$u_p = \frac{u_{px}}{u_0}, \qquad u_e = \frac{u_{ex}}{u_0}, \qquad M_p = \frac{u_0}{c_{p0}}, \qquad M_e = \frac{u_0}{c_{e0}}, \qquad M_A = \frac{u_0}{V_{A0}},$$

where u_0 is the impinging speed at the beginning of the transition ($x = -\infty$), and the subscript 0 refers to values there. We shall call the solution of (26) for u_e as a

https://doi.org/10.1017/S0022377801001076 Published online by Cambridge University Press

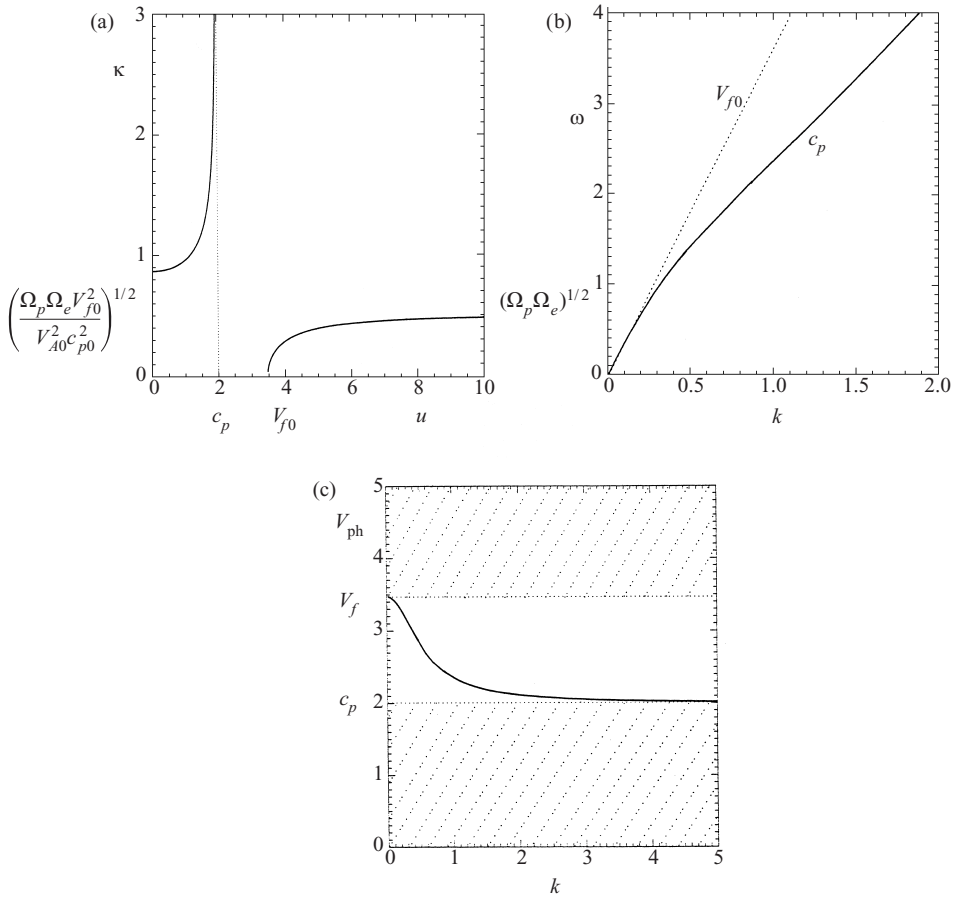


Figure 1. (a) The exponent κ of the stationary-wave dispersion equation as a function of flow speed. Solitons can only exist in the regions $u_0 < c_p$ and $u_0 > V_{f0}$, where $\kappa^2 > 0$. (b) The diagnostic diagram for propagating-wave solutions. (c) The associated phase speed $V_{\rm ph}$ as a function of k. The hatched regions where $V_{\rm ph}$ is imaginary correspond to where solitons may exist.

function of u_p, which defines a locus in the (u_e, u_p) plane, the momentum hodograph of the system. This locus has two asymptotes ($u_e \to \infty$) where the left-hand side, $L(u_p)$ say, takes the value given by

$$L(u_p) \equiv u_p - 1 + \frac{1}{\gamma_p M_p^2}\left(\frac{1}{u_p^{\gamma_p}} - 1\right) = \frac{1}{\gamma_e M_e^2} + \frac{1}{2M_A^2}. \tag{27}$$

The lower and upper asymptotes u_{pl} and u_{pu} are given approximately by

$$u_{pl} \approx \frac{1}{\left(\dfrac{\gamma_p M_p^2}{\gamma_e M_e^2} + \dfrac{\gamma_p M_p^2}{2M_A^2}\right)^{1/\gamma}}, \qquad M_p \gg 1, \qquad M_f > 1, \tag{28a}$$

$$u_{pu} \approx 1 + \frac{1}{\gamma_e M_e^2} + \frac{1}{2M_A^2}, \qquad M_p \gg 1, \qquad M_f > 1, \tag{28b}$$

https://doi.org/10.1017/S0022377801001076 Published online by Cambridge University Press

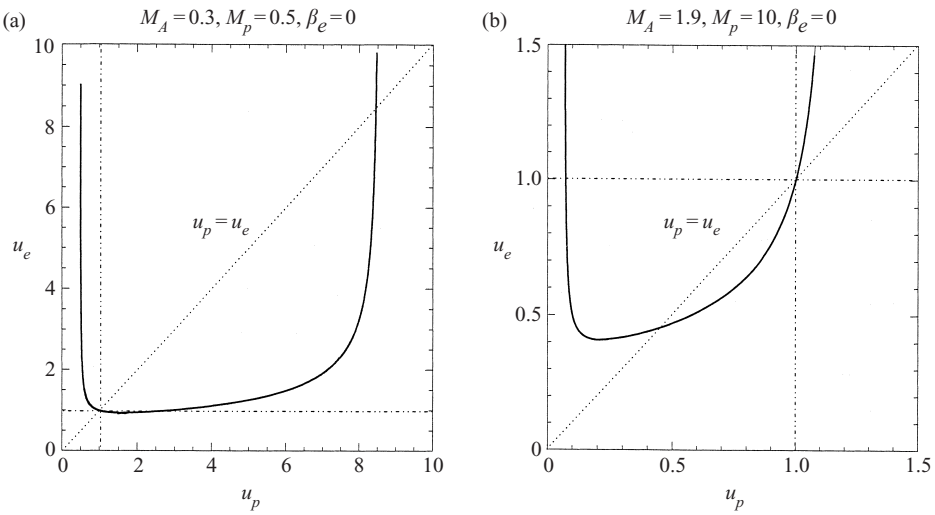


Figure 2. The momentum hodograph as the locus in the (u_e, u_p) plane on which the x component of total momentum is conserved: (a) $M_p < 1$; (b) $M_f > 1$. The u_e asymptotes at $u_p = u_{pl}$ and u_{pu} mark the blocking lines of u_p. Solutions of the structure equation evolve along the right and left branches of the locus from the initial point $(1, 1)$. See the text for a more complete description.

$$u_{pl}^{-1} \approx \left[\gamma_p M_p^2 \left(\frac{1}{\gamma_e M_e^2} + \frac{1}{2M_A^2}\right)\right]^{1/\gamma}, \qquad M_p \ll 1, \qquad M_f \ll 1, \tag{29a}$$

$$u_{pu} \approx \frac{1}{\gamma_p M_p^2} + \frac{1}{\gamma_e M_e^2} + \frac{1}{2M_A^2}, \qquad M_p \ll 1, \qquad M_f \ll 1. \tag{29b}$$

The electron speed u_e possesses a minimum value where $\partial L/\partial u_p = 0$, which occurs where

$$u_p = 1/M_p^{2/\gamma_p + 1}, \tag{30}$$

since

$$\frac{\partial L}{\partial u_p} = 1 - \frac{1}{M_p^2 u_p^{\gamma_p + 1}}. \tag{31}$$

The speed given by (30) corresponds to where the local proton speed equals the proton acoustic speed. This reflects a characteristic property of a Bernoulli-like momentum flux, which always displays a minimum where the flow speed equals the local sound speed. Therefore, using these properties, namely that there are two asymptotes for u_e, a minimum in u_e occurring at the proton acoustic speed, and that the curve must go through the initial point $(1, 1)$ with a slope given by

$$\frac{du_e}{du_p} = \left(1 - \frac{1}{M_p^2}\right) \Big/ \left(\frac{1}{M_e^2} + \frac{1}{M_A^2}\right), \tag{32}$$

the momentum hodograph is readily constructed.

Figure 2 shows the hodograph for the cases (a) $M_p < 1$ and (b) $M_f > 1$ that correspond to the regions of Mach number space in which soliton solutions may exist. In the subsonic case (a), the transition can evolve from the initial point $(1, 1)$ either to the left $(u_p < 1)$ or to the right $(u_p > 1)$. In the former situation,

https://doi.org/10.1017/S0022377801001076 Published online by Cambridge University Press

the protons are decelerated continuously to the limit u_{pl} while the electrons are accelerated ($u_e \to \infty$ as $u_p \to u_{pl}$) to their left asymptote. In the superfast case $M_f > 1$ (b), the transition can again evolve from the initial point either to the left ($u_p < 1$) or the right ($u_p > 1$). In the former situation, the protons and electrons are both decelerated until the proton sonic point is reached, where the electrons are now accelerated with $u_e \to \infty$ and the protons are decelerated to a limiting value u_{pl}. We shall see subsequently that only this branch of the momentum hodograph can be used to construct soliton solutions.

6. The energy integral of the structure equation

In its normalized form, the structure equation (22) may be written as

$$u_e u_p \frac{dY}{dx} = u_e - u_p, \tag{33a}$$

$$Y = u_e u_p \left(1 - \frac{1}{M_p^2 u_p^{\gamma_p+1}}\right) \frac{du_p}{dx}, \tag{33b}$$

in which the spatial coordinate is normalized to the lower-hybrid length scale $l = u_0(\Omega_p \Omega_e)^{-1/2}$. This system integrates immediately to yield

$$\frac{Y^2}{2} = \int_1^{u_p} (u_e - u_p)\left(1 - \frac{1}{M_p^2 u_p^{\gamma_p+1}}\right) du_p = E(u_p), \quad \text{say.} \tag{34}$$

The first integral can be evaluated as follows:

$$\begin{aligned} I_e &= \int_1^{u_p} u_e \left(1 - \frac{1}{M_p^2 u_p^{\gamma_p+1}}\right) du_p = \int_1^{u_p} u_e \frac{\partial L}{\partial u_p}\, du_p = \int_1^{u_p} u_e\, dL \\ &= \int_1^{u_e} u_e \left(\frac{1}{M_e^2 u_e^{\gamma_e+1}} - \frac{1}{M_A^2 u_e^3}\right) du_e \\ &= \frac{1}{M_A^2}\left(1 - \frac{1}{u_e}\right) + \frac{1}{M_e^2(\gamma_e - 1)}\left(1 - \frac{1}{u_e^{\gamma-1}}\right). \end{aligned} \tag{35}$$

The second, third and fourth steps follow from (31) and the derivative of the momentum hodograph, $\partial L/\partial u_e$, (27). The second integral follows in the form

$$I_p = \int_1^{u_p} u_p \left(1 - \frac{1}{M_p^2 u_p^{\gamma_p+1}}\right) du_p = \frac{1}{2}(u_p^2 - 1) + \frac{1}{(\gamma_p - 1)M_p^2}\left(\frac{1}{u_p^{\gamma_p-1}} - 1\right). \tag{36}$$

Hence the integral $E(u_p)$ may be written as

$$\begin{aligned} E(u_p) = \frac{1}{M_A^2}\left(1 - \frac{1}{u_e}\right) + \frac{1}{M_e^2(\gamma - 1)}\left(1 - \frac{1}{u_e^{\gamma_e-1}}\right) + \frac{1}{2}(1 - u_p^2) \\ + \frac{1}{(\gamma_p - 1)M_p^2}\left(1 - \frac{1}{u_p^{\gamma_p-1}}\right). \end{aligned} \tag{37}$$

https://doi.org/10.1017/S0022377801001076 Published online by Cambridge University Press

This expression is readily interpreted as the change between the incoming energy flux and that at any point in the transition (in normalized form). The first term on the right-hand side is the change in the Poynting flux, the second term is the change in the flux of electron enthalpy, the third term is the change of kinetic energy flux of the protons in the x direction, and the last term is the difference in the proton enthalpy flux. The overall change in this energy flux is balanced by the term $\frac{1}{2}Y^2$, see (34), which represents the flux of the kinetic energy associated with the transverse deflections of the protons and electrons in the transition. Thus (34) expresses conservation of total energy flux – a fact that we might have written down at the outset. Nevertheless, it is interesting to note how its 'derivation' follows from the second-order structure equation and the hodograph. Therefore the structure equation reduces to a first-order differential equation for u_p:

$$\frac{du_p}{dx} = \frac{\pm\sqrt{2}E^{1/2}(u_p)}{u_p u_e(1 - 1/M_p^2 u_p^{\gamma_p+1})}. \tag{38a}$$

Alternatively the equivalent first-order differential equation for B is

$$\frac{dB}{dx} = \frac{\mp\sqrt{2}E^{1/2}(B)}{u_p\left(\dfrac{1}{M_A^2} + \dfrac{B^{\gamma_e-2}}{M_e^2}\right)}. \tag{38b}$$

Before discussing the possible structures embedded in (38), we first make contact with the classical work on solitons in a cold magnetized plasma (Adlam and Allen 1958; Vedenov et al. 1961; Sagdeev 1966). In the cold limit, $M_e^2 = M_p^2 = \infty$, the momentum hodograph (26) simplifies to

$$u_p - 1 = \frac{1}{2M_A^2}\left(1 - \frac{1}{u_e^2}\right) = \frac{1}{2M_A^2}(1 - B^2). \tag{39}$$

The structure equation (as an 'energy integral' equation (38a)) also simplifies somewhat to

$$u_e u_p \frac{du_p}{dx} = \pm\sqrt{2}E^{1/2}(u_p), \tag{40}$$

where E now becomes

$$E = \frac{1}{M_A^2}\left(1 - \frac{1}{u_e}\right) + \frac{1}{2}(1 - u_p^2) = \frac{(B-1)^2}{2M_A^2}\left[1 - \frac{(B+1)^2}{4M_A^2}\right], \tag{41}$$

in which the latter form follows from $u_e = B^{-1}$ and the momentum equation (39). The corresponding differential equation for B is

$$\frac{dB}{dx} = \frac{\pm M_A(B-1)\left[1 - \dfrac{(B+1)^2}{4M_A^2}\right]}{1 + \dfrac{1}{2M_A^2}(1 - B^2)}. \tag{42}$$

For $M_A < 2$, $dB/dx = 0$ at $B \equiv B_m = 2M_A - 1$, which is smaller than the value of B ($B_c = (1 + 2M_A^2)^{1/2}$) at which $dB/dx = \infty$, we then obtain the classical soliton of Adlam and Allen (1958).

However, for $M_A > 2$, $dB/dx = \infty$ at $B = B_c$, which is now less than B_m, with the result that a solution can be constructed by joining the mirror image of the integral curve about the reflection point. This gives rise to cusp-like soliton

https://doi.org/10.1017/S0022377801001076 Published online by Cambridge University Press

structures shown in Fig. 5(b) in which, near the centre ($x = 0$, say) of the wave,

$$B \sim B_c - x^{1/2}, \tag{43}$$

$$u_p \sim \frac{B_c}{M_A}(B_c - B). \tag{44}$$

Because $u_p \to 0$ as $B \to B_c$ there is an infinite spike in the proton density. Nevertheless, the charge-separation electric field associated with this spike is still small ($\sim x^{1/2}$) because the singularity is integrable. However, such a cusp-like profile in B implies the introduction of current sheets, and it is not obvious that such structures can stably exist.

7. The effect of plasma pressure on soliton structure

Here we examine the structure of stationary waves, including the effect of plasma pressure, which manifests itself through the proton Mach number M_p and the fast Mach number M_f. The integral curves of the equivalent differential equations (38) can be constructed from our knowledge of the behaviour of the momentum hodograph and energy flux integral. To this end, it is useful to expand E in powers of $u_p - 1 \equiv \delta$ to obtain (up to δ^3)

$$E(u_p) \approx a_2\delta^2 + a_c\delta^3 + \dots, \tag{45a}$$

in which

$$a_2 = \tfrac{1}{2}(1 - M_p^{-2})[M_f^2(1 - M_p^{-2}) - 1], \tag{45b}$$

$$a_3 = -\frac{\gamma + 1}{3M_p^2} + \tfrac{1}{2}M_{Ae}^2(1 - M_p^{-2})[(\gamma + 1)M_p^{-2} + M_{Ae}^{-2}(1 - M_p^{-2})^2]. \tag{45c}$$

Here $M_{Ae}^2 = u_0^2/(c_e^2 + V_{A0}^2)$. The differential equation (38a) linearizes to

$$\frac{d\delta}{dx} = m\delta, \tag{46a}$$

$$m = \pm\left[\frac{2a_2}{(1 - M_p^{-2})^2}\right]^{1/2} = \pm\left[\frac{M_{Ae}^2(1 - M_p^{-2}) - 1}{1 - M_p^{-2}}\right]^{1/2}. \tag{46b}$$

This admits exponential solutions $\exp(\pm mx)$, where the exponent m given by (45b) is the normalized equivalent of the stationary-wave dispersion relation (24a), requiring $M_p < 1$ or $M_f > 1$ for growing or decaying solutions at $x = \mp\infty$. Note that $M_{Ae}^2(1 - M_p^{-2}) > 1$ is equivalent to $M_f > 1$, where $M_f = u_0(c_p^2 + c_e^2 + V_A^2)^{-1/2}$ is the fast Mach number. Thus all integral curves of (38a) emanate from $u_p = 1$ in an exponential fashion. The expansion (45a) shows that, in addition to E having a double zero at the initial point, it also has a simple zero (which corresponds to an equilibrium point of differential equation), where δ is given by

$$u_p - 1 = \delta = -\frac{a_2}{a_3}. \tag{47}$$

For weakly nonlinear structures, this gives an approximation to the strength of the soliton, which, since $a_2 > 0$, can either be a compression $\delta < 0$ (requiring $a_3 > 0$) or a rarefaction $\delta > 0$ ($a_3 < 0$). For example, in the cold case ($M_p = \infty$) and $M_f \approx 1$

https://doi.org/10.1017/S0022377801001076 Published online by Cambridge University Press

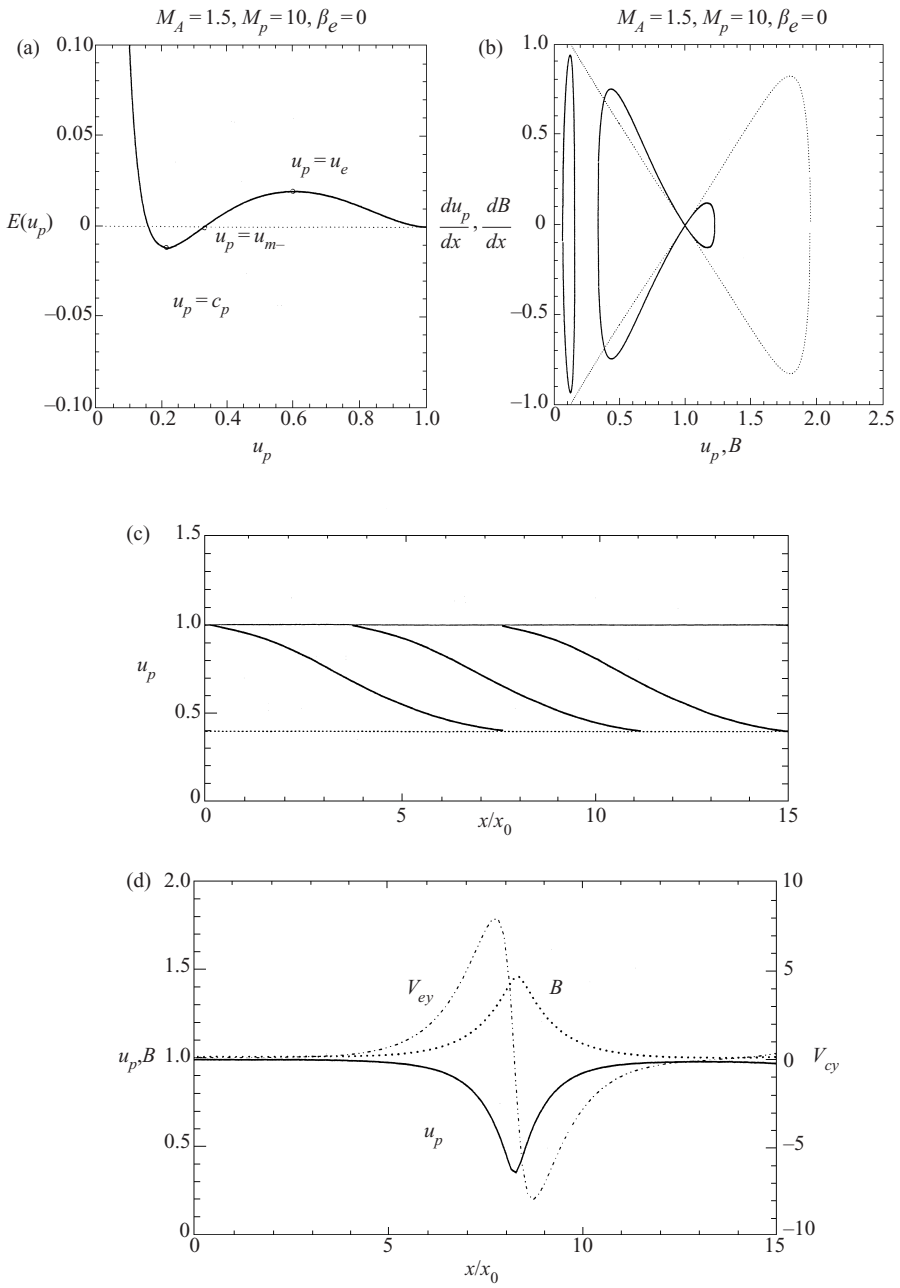


Figure 3. (a) The energy $E(u_p)$ as a function of u_p for $M_f > 1$. (b) The associated phase curves in the $(du_p/dx, u_p)$ plane (solid lines) and $(dB/dx, B)$ plane (dotted lines). The compression soliton is represented by the closed curve in $u_p < 1$ and the broken closed line in $B > 1$. The other closed curve cannot be reached from the initial point without the introduction of discontinuities. (c) The integral curves in (u_p, x) space and (B, x) space, with the associated flow deflection. (d) Soliton solutions in u_p and B constructed from the mirror images of the integral curves about the equilibrium point.

https://doi.org/10.1017/S0022377801001076 Published online by Cambridge University Press

(but > 1), we have the compression

$$u_{p\,\min} \approx 1 - \frac{M_f^2 - 1}{M_f^4}, \tag{48a}$$

$$B_{\max} \approx 1 + \frac{M_f^2 - 1}{M_f^2}; \tag{48b}$$

whereas in the case $M_p < 1$ ($M_p^2 = 1 - \epsilon, \epsilon \ll 1$), we have a weak expansion in u_p given by

$$u_{p\,\max} \approx 1 + \frac{3\epsilon}{2(\gamma + 1)}, \tag{49a}$$

with an associated very weak compression in B:

$$B_{\max} \approx 1 + \frac{3}{2}\frac{M_f^2\epsilon^2}{(\gamma + 1)}. \tag{49b}$$

Equation (38a) possesses different types of integral curves, depending upon the location of the equilibrium points ($du_p/dx = 0$ at the zeros of $E(u_p)$) and the asymptotes of the hodograph (where $u_e \to \infty$) and the reflection points ($du_p/dx = \infty$ at the proton sonic point). In order to elucidate the properties of the integral curves, we examine the behaviour of $E(u_p)$, from which we can construct the phase curves in the $(du_p/dx, u_p)$ and $(dB/dx, B)$ planes.

For example, Fig. 3(a) shows $E(u_p)$ as a function of u_p for $M_A > 1$ ($M_A = 1.5$) and $M_p = 10$. $E(u_p)$ possesses a zero at $u_p = u_{m-}(\approx 0.33) > M_p^{2/(\gamma+1)} \approx 0.215$). Hence the equilibrium point is reached before the flow becomes locally 'sonic'. The phase curves of this soliton structure are displayed in Fig. 3(b). In this case, the integral curves have the form shown in Fig. 3(c). The corresponding soliton solutions are shown in Fig. 3(d) as mirror-image reflections of the integral curves by changing the sign of the slope du_p/dx at the equilibrium point. The associated compression in B is also shown in Fig. 3(d). The deflection of the electron flow in the y direction shows that it reaches a maximum where the line $u_p = u_e$ intersects the hodograph (see Fig. 2b). In the phase plane, there are also rarefaction solutions ($u_p > 1$, $B < 1$). However, note that the deflection of the electron flow is given by

$$\frac{du_{ey}}{dx} = \left(\frac{m_p}{m_e}\right)^{1/2}\left(\frac{1}{u_p} - \frac{1}{u_e}\right). \tag{50}$$

Because the intersection between the line $u_e = u_p$ and the hodograph in the rarefaction branch $u_p > 1$ occurs after the equilibrium and sonic points, we cannot construct a soliton solution in which the deflection is an odd function of x going to zero in the centre of the wave and at each end ($x = \mp\infty$) (see the form of deflection shown in Fig. 3d).

It is interesting to note that an increase in M_A (at the same M_p) can lead to a dramatic change in the behaviour of the energy $E(u_p)$ curve. Figure 4(a) shows that in the case $M_A = 1.6$ and $M_p = 10$, $E(u_p)$ no longer has a zero in $u_p < 1$. In this case, the only equilibrium point is the u_e asymptote of the hodograph, which, however, occurs at a smaller value of u_p than the local sonic point at which du_p/dx is infinite. The corresponding phase curves are shown in Fig. 4(b). In this case, it is not possible to construct a classical soliton (i.e. a mirror-image reflection about the equilibrium point) because of the infinity of du_p/dx at the sonic point. However,

https://doi.org/10.1017/S0022377801001076 Published online by Cambridge University Press

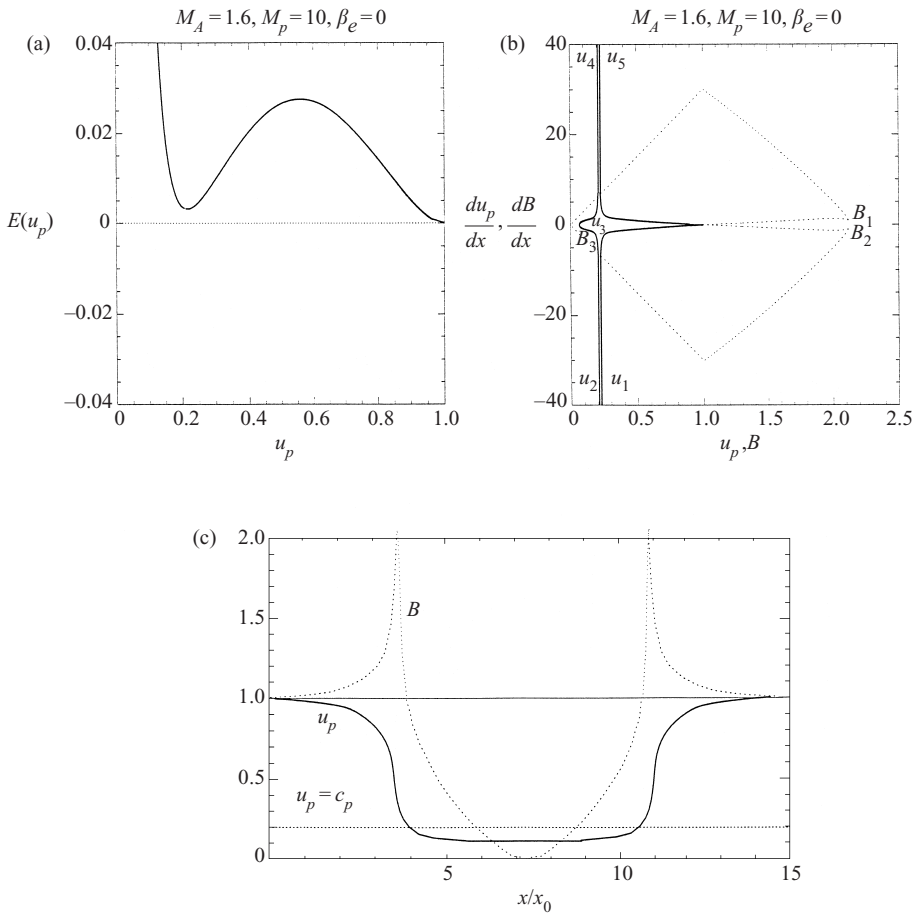


Figure 4. (a) A small change in the Alfvén Mach number (and M_f) leads to $E(u_p)$ no longer having a zero in the compression branch $u_p < 1$. (b) The corresponding phase curves, showing that the proton sonic point ($du_p/dx = \infty$) is reached before the equilibrium point associated with $u_e \to \infty$. (c) A possible structure in which B has two cusps and a deep minimum obtained by change of sign of the derivatives introduced at the reflection points, thus permitting a supersonic–subsonic transition.

it is possible to construct an interesting structure in which we reflect (i.e. change the sign of the derivatives) about the sonic point. The corresponding phase trajectories in the $(du_p/dx, u_p)$ and $(dB/dx, B)$ planes are (1, u_1, u_2, u_3, u_4, u_5, 1) and (1, B_1, B_2, $B_3 = 0$, B_1, B_2, 1) respectively (Fig. 4b). One possible such structure is shown in Fig. 4(c) in which changes of sign are introduced at the reflection points and the equilibrium point at the centre of the wave. In this structure, the profile of B has two cusps and a deep minimum. This, of course, implies the presence of current sheets at the location of the cusps. Clearly, in the region of the deep minimum of B, the proton pressure (proportional to $u_p^{-\gamma}$) is correspondingly high where the proton speed is low. Structures of this form have been observed ahead of the Earth's bow shock, and have been called 'hot anomalies' (Paschmann et al. 1988; Thomsen et al. 1986, 1988; Schwartz et al. 1988).

Let us now examine the sub-proton-acoustic case ($M_p < 1$), which necessarily implies that $M_f < M_p < 1$. An example of the behaviour of $E(u_p)$ in this case is

https://doi.org/10.1017/S0022377801001076 Published online by Cambridge University Press

shown in Fig. 5(a) (for which the corresponding hodograph is displayed in Fig. 2a). The equilibrium point, occurring at $u_p = u_{m+} \approx 2$, corresponds to a rarefaction in u_p but a compression in B. However, in this case, the sonic point $u_p = M_p^{2/(\gamma+1)}$ (≈ 1.59 for $\gamma = 2$) is reached before the equilibrium point, and the integral curves are of the form shown in Fig. 5(c). The phase curves are shown in Fig. 5(b). In the case of M_p near unity ($M_p^2 = 1 - \epsilon$, $\epsilon \ll 1$) the sonic point occurs at

$$u_p = 1 + \frac{\epsilon}{\gamma + 1}, \tag{51}$$

which is indeed smaller than the equilibrium point (49a). This fact, along with the property that the line $u_e = u_p$ intersects the hodograph at values of u_p between the sonic point and the right asymptote, implies that it is not possible to construct smooth classical soliton solutions in which the deflection is an odd function of x. However, in the same way as before, we can construct the structure shown in Fig. 5(d) by switching signs of derivatives at the reflection and equilibrium points. In this case, we have a rarefaction in u_p accompanied by a compression (rather weak) in B, in accordance with (48) appropriate to the weak case. The phase trajectories in the (du_p/dx, u_p) and (dB/dx, B) planes, (1, u_1, u_2, u_3, u_4, 1) and (1, B_1, B_2, B_3, B_1, B_2, 1), shown in Fig. 5(b), correspond to the structure shown in Fig. 5(c), in which one must effect jumps at the reflection points ($du_p/dx = \infty$) and the equilibrium point ($du_p/dx = 0$). There is a compression solution for u_p (and a rarefaction in B). But again, because there is no way in which we can have an odd deflection, a soliton pulse cannot be constructed from this branch of the hodograph.

The sample of results for $M_f > 1$ can be placed in a more general context in the following way. In the case $M_f > 1$ (and, of course, $M_p > 1$), the disappearance of the roots of $E(u_p) = 0$, $u_p < 1$, for a certain combination of the Mach-number parameters corresponds to the maximum attainable compression in B and the associated maximum speed of the soliton (measured by M_f). To see this, note that

$$\frac{dE(u_p)}{du_p} = \left(1 - \frac{1}{M_p^2 u_p^{\gamma_p+1}}\right)(u_e - u_p). \tag{52}$$

Hence $dE(u_p)/du_p$ is zero at the proton sonic point ($u_p = M_p^{-2/(\gamma+1)}$) and the 'charge-neutral' point $u_e = u_p$. Therefore the zeros of $E(u_p)$ (other than the double zero at the initial point) interlace the points of zero gradient (see Fig. 6). A critical case occurs where a double root occurs at the proton sonic point; that is,

$$E(u_p) = \frac{dE}{du_p} = 0 \quad \text{at } u_p = M_p^{-2/(\gamma+1)}. \tag{53}$$

This yields the following relation between M_{Ae} and M_p:

$$M_{Ae}^2 = -\frac{2[e_p + L(u_p)]}{e_p^2} \tag{54a}$$

where

$$e_p = \frac{1}{2}(1 - u_p^2) + \frac{1}{(\gamma_p - 1)M_p^2}\left(1 - \frac{1}{u_p^{\gamma_p - 1}}\right), \tag{54b}$$

$$L(u_p) = u_p - 1 + \frac{1}{\gamma M_p^2}\left(\frac{1}{u_p^{\gamma_p}} - 1\right), \tag{54c}$$

https://doi.org/10.1017/S0022377801001076 Published online by Cambridge University Press

https://doi.org/10.1017/S0022377801001076 Published online by Cambridge University Press

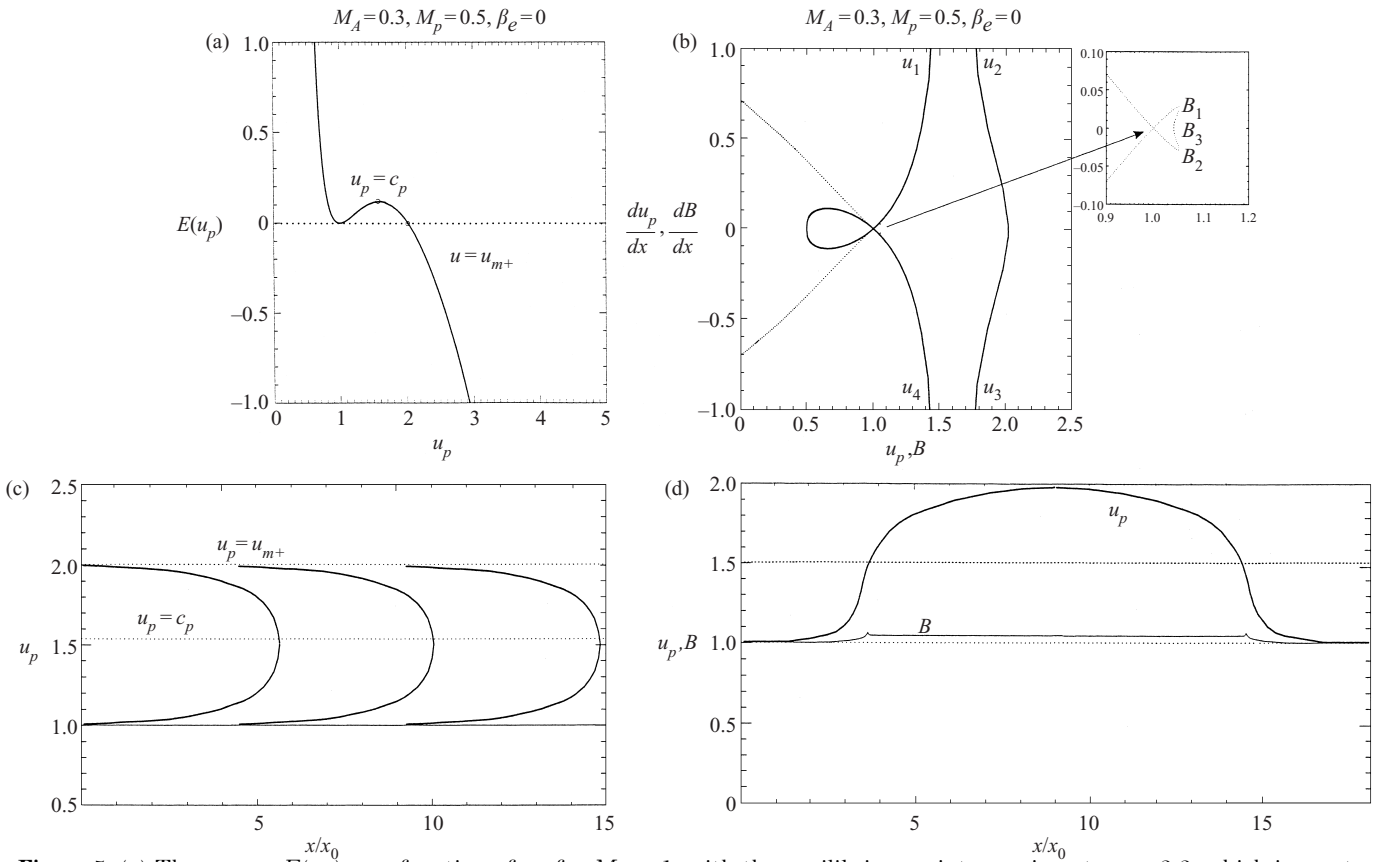


Figure 5. (a) The energy $E(u_p)$ as a function of u_p for $M_p < 1$, with the equilibrium point occuring at $u_p \approx 2.2$, which is greater than the sonic proton speed ($u_p \approx 1.59$). (b) The corresponding phase curves. (c) The integral curves (u_p, x), showing choked flow at the proton sonic point. (d) A possible structure in which B has two cusps obtained by a change of sign of the derivatives introduced at the points B_1, B_2 and u_1, u_3, thus permitting a subsonic–supersonic transition.

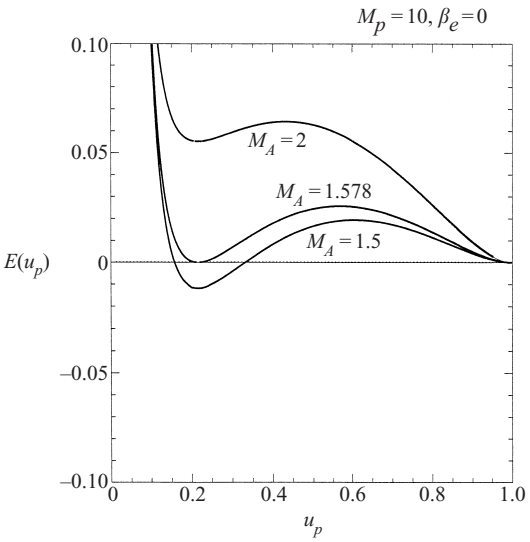


Figure 6. The energy $E(u_p)$ as a function of u_p for Mach numbers below critical, critical and above critical. At the critical Mach number, $E(u_p)$ has a double zero (at $u_p \approx 0.2$) and above the critical Mach number, $E(u_p)$ has no zeros (other than at the initial point).

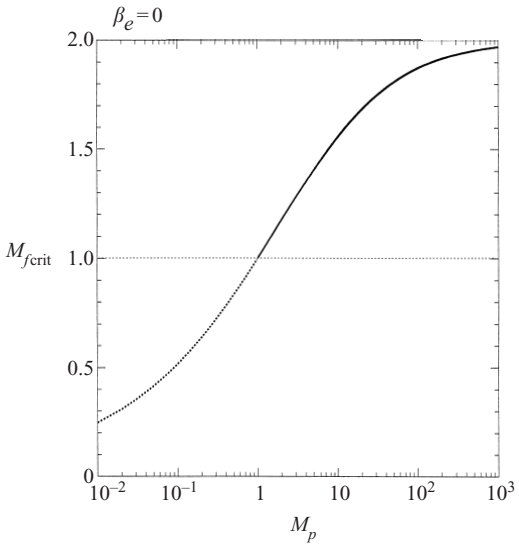


Figure 7. The critical fast Mach number $M_{f\text{crit}}$ as a function of the proton acoustic Mach number M_p.

evaluated at

$$u_p = M_p^{-2/(\gamma+1)}. \tag{54d}$$

This relation for M_{Ae} can be used to give the critical fast Mach number $M_{f\text{crit}}$ as a function of M_p, i.e.

$$M_{f\text{crit}}^2 = \frac{M_p^2}{1 + M_{Ae}^2/M_p^2}. \tag{55}$$

https://doi.org/10.1017/S0022377801001076 Published online by Cambridge University Press

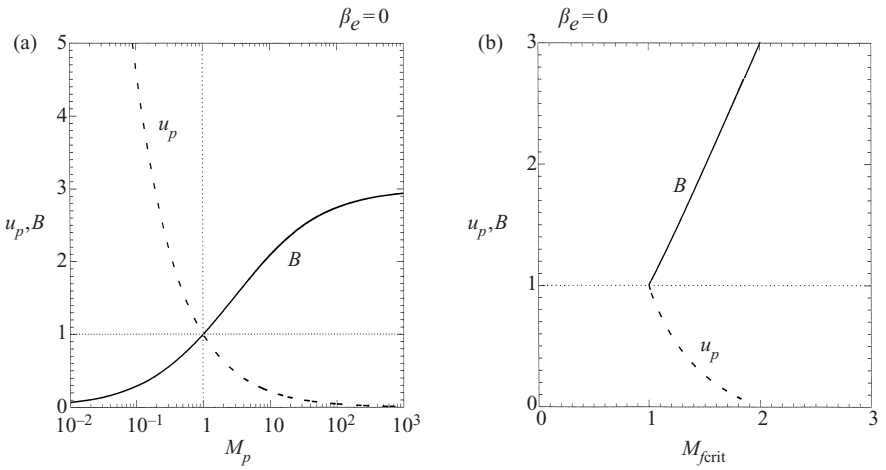


Figure 8. The maximum compression in B and u_p as functions of (a) M_p and (b) $M_{f\mathrm{crit}}$.

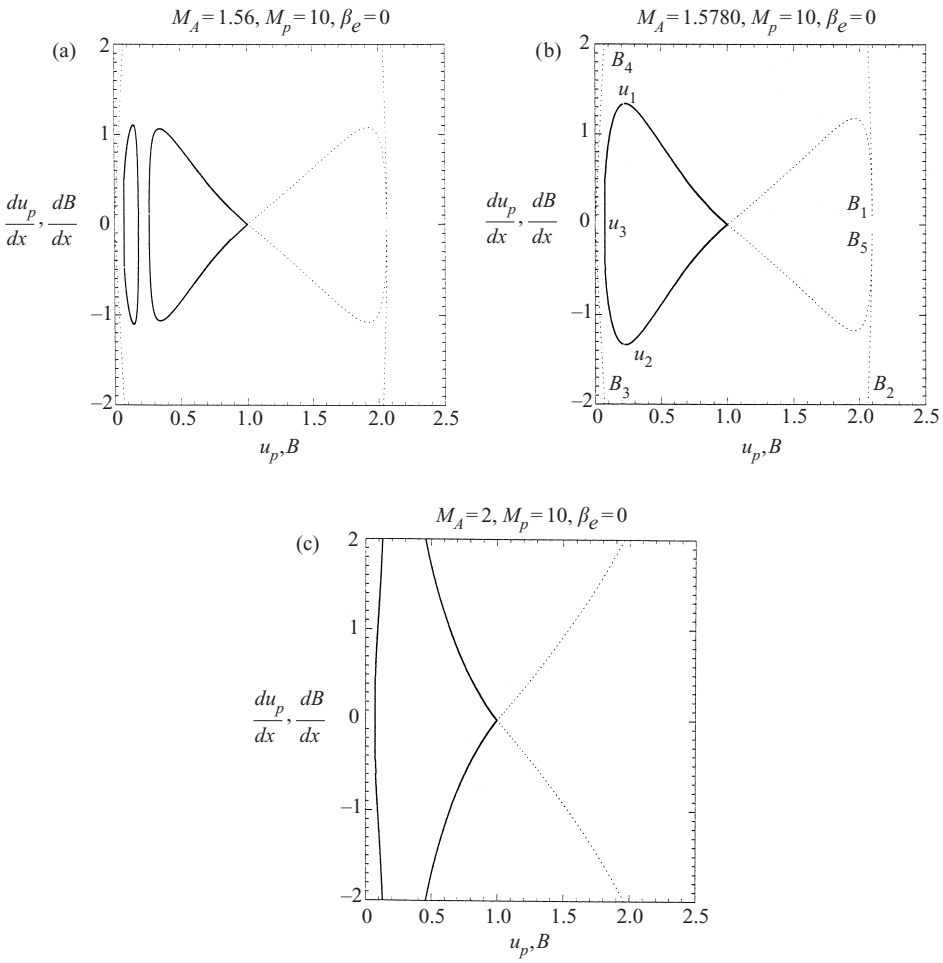


Figure 9. The phase curves for (a) $M_f < M_{f\mathrm{crit}}$, (b) $M_f = M_{f\mathrm{crit}}$ and (c) $M_f > M_{f\mathrm{crit}}$.

https://doi.org/10.1017/S0022377801001076 Published online by Cambridge University Press

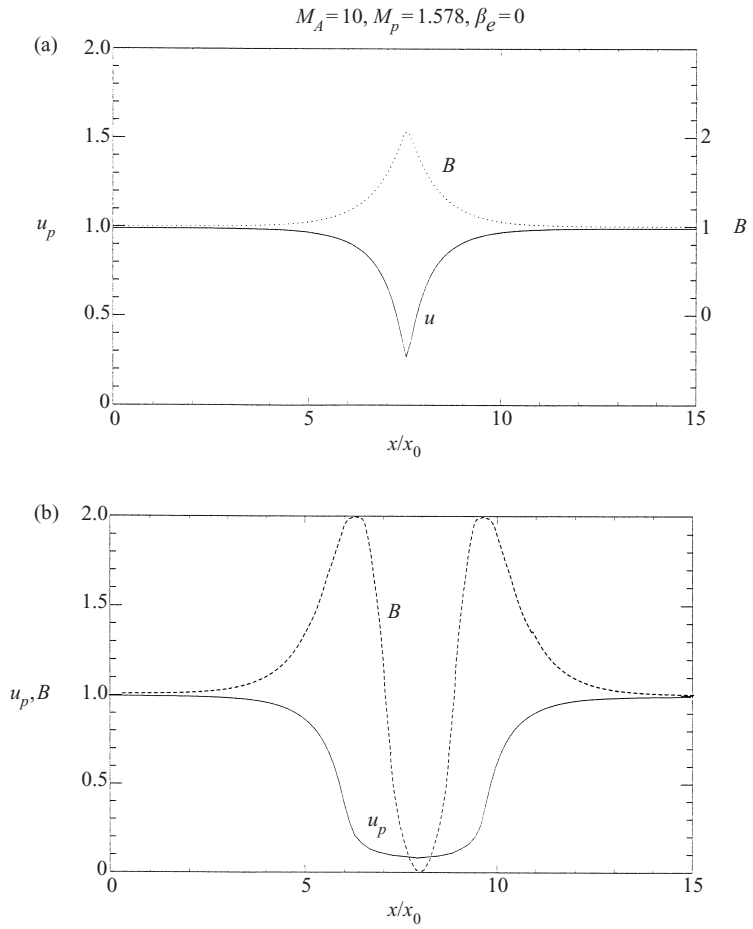


Figure 10. (a) Single-humped critical compressive soliton with cusplike behaviour in u_p. (b) Double-humped compressive–rarefactive critical soliton involving a smooth supersonic–subsonic transition in the proton flow.

The corresponding maximum compression is

$$B_{\max} = 1 + M_{Ae}^2 e_p(u_p), \tag{56a}$$

or

$$B_{\max} = [1 - 2M_{Ae}^2 L(u_p)]^{1/2} \quad \text{at } u_p = M_p^{-2/(\gamma+1)}. \tag{56b}$$

Figure 7 shows the variation of M_f with M_p. The region $M_p < 1$ is not permitted, since $M_{Ae}^2 < 0$, and in any case we cannot construct smooth solitons in this region. In fact, the double-root condition swaps from the proton sonic point to the charge-neutral point. In general, we conclude that plasma-pressure effects reduce the critical fast Mach number (given by (54) and (55)) to less than 2. The limiting compression $B_{\max}$ and corresponding u_p as functions of M_p and M_f are shown in Fig. 8.

It is interesting to examine in some detail the nature of possible soliton structures at the critical fast Mach number given by (55). The phase curves for the cases $M_f < M_{f\text{crit}}$, $M_f = M_{f\text{crit}}$ and $M_f > M_{f\text{crit}}$ are shown in Fig. 9. Recall that at the critical

https://doi.org/10.1017/S0022377801001076 Published online by Cambridge University Press

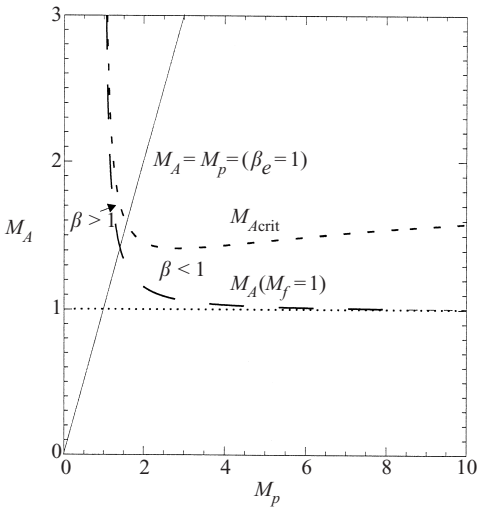


Figure 11. The parameter space (M_A, M_p), showing the regions of low-β solitons and a small region of high-β solitons, which are necessarily very weak.

Mach number, $E(u_p)$ has a double root occurring at the local proton sonic point, with the result that reflection of the mirror image of the integral curves gives rise to the soliton structure shown in Fig. 10(a), in which B reaches a maximum smoothly in the centre of the wave but u_p develops a cusp. In the phase plane (Fig. 10b), the sonic point is reached at $u_p = u_2$, where du_p/dx has a minimum, giving rise to a cusp-like structure (Fig. 10a). However, it is also possible to construct the soliton structure shown in Fig. 10(b) by allowing u_p to go (smoothly) from supersonic to subsonic flow (the phase trajectories are (1, u_2, u_3, u_1, 1) and (1, B_1, B_2, B_3, 0, B_4, B_1, B_5, 1)), which means that we follow the momentum hodograph down to values of u_{pl} (where $u_e \to \infty$, $B \to 0$) and reflect the mirror image about this equilibrium point. In this structure, B (and u_p) develop a deep minimum in the centre of the wave, and this is accompanied by an increase in the proton plasma pressure. This critical soliton structure is the smooth equivalent of the one shown in Fig. 4(c), in which cusps in B are introduced.

It is also interesting to plot in the parameter space (M_A, M_p) (Fig. 11) the regions in which there are low-β ($\beta < 1$) solitons and high-β ($\beta > 1$) solitons. Because $M_f \to 1$ as $M_p \to 1$, this latter region is very limited to M_p slightly greatly than unity and M_A lying between $M_f = 1$ and $M_{A\,\mathrm{crit}}$.

Finally, it is also worth noting that shocklike structures involving the insertion of a plasma subshock in the case $M_f > M_{f\mathrm{crit}}$ can be also constructed. Rather than reflecting the mirror image about the reflection point ($du_p/dx = \infty$ at the proton acoustic point), one can insert a subshock somewhere in the region $M_p > 1$ to achieve $M_p < 1$ downstream in much the same way as gas subshocks are inserted into cosmic-ray shocks (see e.g. Axford et al. 1982) or ion sound subshocks are embedded within a broader magnetic field structure (Kennel et al. 1985).

8. Summary

The properties of the momentum hodograph and the energy integral of the system elucidate the nature of stationary waves propagating perpendicularly to the am-

https://doi.org/10.1017/S0022377801001076 Published online by Cambridge University Press

bient magnetic field in a plasma, including the effects of plasma pressure. It has been shown that the critical fast Mach number M_f has a weak dependence on the proton acoustic Mach number M_p, varying from the value 2 (at large M_p) to unity (as $M_p \rightarrow 1$). At the critical fast Mach number, a soliton may have two possible structures. One is the classical one involving a compression of the magnetic field (accompanied by a corresponding deceleration in the proton flow) followed by its mirror image, which returns the structure to the original state. The other possible structure can be constructed via a smooth supersonic–subsonic transition in the proton flow in which the magnetic field is first compressed and then deeply depressed, with the mirror image returning the wave (flow) to its original state. Waves propagating at speeds in excess of critical may have structures similar to the latter, but with the magnetic field exhibiting cusplike behaviour at the proton sonic point. Other transitions involving a plasma subshock may be constructed in a fashion similar to cosmic-ray shocks or hydromagnetic shocks, in which, in the latter, the final jump takes place through a subshock on length scales finer than the hybrid length scale. Such a transition in which a subshock appears may also be relevant to magnetopause structures where the magnetic field is perpendicular to the flow near its stagnation point.

References

Adlam, J. and Allen, J. 1958 The structure of strong collision-free hydromagnetic waves. *Phil. Mag.* **3**, 448.

Axford, W. I., Leer, E. and McKenzie, J. F. 1982 The structure of cosmic ray shocks. *Astron. Astrophys.* **111**, 317.

Drazin, P. G. 1983 *Solitons.* Cambridge University Press.

Karpman, V. I. 1975 *Nonlinear Waves in Dispersive Media.* Pergamon Press, Oxford.

Kennel, C. F., Edmiston, J. P. and Hada, T. 1985 A quarter century of collisionless shock research. In: *Collisionless Shocks in the Heliosphere: A Tutorial Review* (ed. R. G. Stone and B. T. Tsurutani), p. 1. Geophysical Monograph 34, Washington, DC.

Paschmann, G., Haerendel, G., Sckopke, N. and Mobius E. 1988 Three-dimensional plasma structures with anomalous flow directions near the Earth's bow shock. *J. Geophys. Res.* **93**, 11 279.

Sagdeev, R. Z. 1966 Cooperative phenomena and shock waves in collisionless plasma. In: *Reviews of Plasma Physics*, Vol. 4 (ed. M. A. Leontovich), p. 23. Consultants Bureau, New York.

Schwartz, S. J., Kessel, R. L., Brown, C. C., Woolliscroft, L. J. C., Dunlop, M. W., Farrugia, C. J. and Hall, D. S. 1988 Active current sheets near the Earth's bow shock. *J. Geophys. Res.* **93**, 11 295.

Thomsen, M. F., Gosling, J. T., Fuselier, S. A., Bame, S. J. and Russell, C. T. 1986 Hot diamagnetic cavities upstream from the Earth's bow shock. *J. Geophys. Res.* **91**, 2961.

Thomsen, M. F., Gosling, J. T., Bame, S. J. and Quest, K. B. 1988 On the origin of hot diamagnetic cavities near the Earth's bow shock. *J. Geophys. Res.* **93**, 11 311.

Vedenov, A. A., Velihov, E. P. and Sagdeev, R. Z. 1961 Nonlinear oscillations in rarefied plasma. *Nucl. Fusion* **1**, 82.

https://doi.org/10.1017/S0022377801001076 Published online by Cambridge University Press